Journal of Hazardous Materials 198 (2011) 143–150

Contents lists available at SciVerse ScienceDirect

Journal of Hazardous Materials

journal homepage: www.elsevier.com/locate/jhazmat

Superb fluoride and arsenic removal performance of highly ordered mesoporous aluminas

Wei Li[a,b], Chang-Yan Cao[a], Ling-Yan Wu[a,b], Mao-Fa Ge[a], Wei-Guo Song[a,*]

[a] Key Laboratory for Molecular Nanostructures and Nanotechnology, Institute of Chemistry, Beijing National Laboratory for Molecular Sciences (BNLMS), Chinese Academy of Sciences, Beijing 100190, PR China
[b] Graduate University of Chinese Academy of Sciences, Beijing 100049, PR China

ARTICLE INFO

Article history:
Received 16 February 2011
Received in revised form 5 October 2011
Accepted 6 October 2011
Available online 15 October 2011

Keywords:
Mesoporous aluminas
Fluoride
Arsenic
Adsorption
Water treatment

ABSTRACT

Highly ordered mesoporous aluminas and calcium-doped aluminas were synthesized through a facile and reproducible method. Their fluoride adsorption characteristics, including adsorption isotherms, adsorption kinetics, the effect of pH and co-existing anions were investigated. These materials exhibited strong affinity to fluoride ions and extremely high defluoridation capacities. The highest defluoridation capacity value reached 450 mg/g. These materials also showed superb arsenic removal ability. 1 g of mesoporous alumina was able to treat 200 kg of arsenic contaminated water with a pH value of 7, reducing the concentration of arsenate from 100 ppb to 1 ppb.

1. Introduction

Long-term ingestion of fluoride contaminated water can cause dental and skeletal fluorosis [1,2] while intake of arsenic contaminated water can lead to arsenicosis, various types of cancers and blackfoot disease [3,4]. The World Health Organization (WHO) has set the guideline values of 1.5 mg L^{-1} for fluoride [2] and 0.01 mg L^{-1} for arsenic [5] in drinking water. However, the concentrations of fluoride and/or arsenic in groundwater in China, India, Bangladesh area, Central Africa, USA and South America exceed these values, threatening the health of millions of people [6].

Many defluoridation and arsenic removal methods have been developed [3,7]. These methods include chemical precipitation [8–13], ion exchange [14,15], membrane process [16–19], adsorption technique [1,2,20,21], Donnan dialysis [22,23] and electrodialysis [24]. Each technology may be suitable for certain conditions, such as the population of resident, the electricity supply and funds. Among these methods, the adsorption technique is perhaps the most extensively adopted one because of its simplicity and low cost. While other technologies require complicated setups, the simplest adsorption unit may require only a filter, making it ideal for small scale water treatment units for households or small villages. A wide range of adsorption materials have been reported for fluoride or arsenic removal, such as activated alumina [25–27], activated carbon [28], hydroxyapatite [20,29], alum [30], lime [31], red mud [32], bone char [33], rare earth oxides [34], hydrous ferric oxide [35,36], Mg/Al layered double hydroxide [37,38] and zeolite [39]. However, most of these adsorbents have low defluoridation or arsenic removal capacities in treating complicated groundwater. It is still a challenge to develop better adsorbents with superior adsorption capacities for fluoride or arsenic.

Porous materials are known for their high adsorption capacities [40,41]. The large surface areas, narrow pore-size distributions and highly uniformly channels are favorable features for removing fluoride ions and arsenic species. Due to its large-scale production, high affinity and selectivity towards fluoride and arsenic, commercial activated alumina is perhaps the most frequently used material for removal of fluoride and arsenic from drinking water. The defluoridation capacity of activated alumina is only about 7.6 mg/g [25] and its arsenic removal capacity is 9.0 mg/g [26]. Mesoporous alumina is a new generation of porous alumina. Lee et al. found that the adsorption capacity of mesoporous aluminas for fluoride was 14.3 mg/g [2]. Kim et al. [41] used a similar method to prepare mesoporous γ-alumina, whose maximum uptake capacity for As (V) was 121 mg/g. However, though the maximum adsorption capacities of many adsorbents for arsenic were reported to be high, many of them showed quite low removal capacities at low arsenic concentrations, e.g. 500 ppb and the arsenic concentrations of most arsenic contaminated underground water supply are usually lower than 500 ppb.

* Corresponding author. Tel.: +86 10 62568158; fax: +86 010 62557908.
E-mail address: wsong@iccas.ac.cn (W.-G. Song).

0304-3894/$ – see front matter © 2011 Elsevier B.V. All rights reserved.
doi:10.1016/j.jhazmat.2011.10.025

In this study, we synthesized highly ordered mesoporous aluminas and calcium-doped aluminas through a reproducible and high-yield method and investigated their adsorption characteristics for fluoride and arsenic. These mesoporous alumina materials exhibited excellent fluoride and arsenic removal capacities. The best sample, Ca-doped mesoporous alumina showed a maximum fluoride removal capacity of 450 mg/g and excellent selectivity towards fluoride ion. In addition, these highly ordered mesoporous aluminas exhibited superior arsenic removal ability at low initial arsenic concentrations (i.e. 100 ppb). 1 g of these materials can treat 200 kg of arsenic contaminated water, reducing the concentration of arsenate from 100 ppb to 1 ppb, resulting in an impressive arsenic adsorption capacity of 20 mg/g for practical application.

2. Experimental

2.1. Chemicals and materials

Pluronic P123 (M_{av} = 5800) and sodium arsenite ($NaAsO_2$) were purchased from Sigma–Aldrich. Aluminum isopropoxide (98+ wt%), calcium nitrate tetrahydrate and sodium hydrogen arsenate heptahydrate were purchased from Alfa Aesar. Anhydrous ethanol and nitric acid were purchase from Beijing Chemical Reagents. Sodium fluoride (ACS grade >99%) was purchased from Acros Organic. All chemicals were used as received. Deionized water used in all of the experiments was prepared using Milli-Q water by Milli-Q system (Millipore, Bedford, MA).

2.2. Synthesis of adsorbents

The highly ordered mesoporous aluminas and composites were synthesized by a sol–gel route with block copolymers as soft templates [42–44]. In a typical synthesis procedure, 2.0 g of triblock copolymer Pluronic P123 was dissolved in 40.0 mL of anhydrous ethanol at room temperature and stirred for 1 h. Then 3.2 mL of 67 wt% nitric acid and 4.08 g (20 mmol) of aluminum isopropoxide were added into the above solution with vigorous stirring. After being stirred for 5 h, the solvent was evaporated at 60 °C for 48 h in air under static condition. The resulting powder samples were calcined at 400 or 900 °C, respectively, for 4 h in air. Ordered mesoporous aluminas and calcium oxide composites were synthesized using the above-mentioned procedure, with addition of desired amounts of calcium nitrates to the synthesis mixtures. The samples were labeled to indicate the loading of Ca in the composite as well as other synthesis conditions (i.e. temperature).

2.3. Batch adsorption tests

All the batch fluoride and arsenate adsorption experiments were carried out at room temperature (298 K) using polyethylene (PE) vessels. The stock solution of fluoride (1000 mg L^{-1}) was prepared and then diluted to desired concentrations. The initial pH value of all fluoride solution is fixed at 6.5. Then 0.01 g of the adsorbent sample was added to 100 mL of the above fluoride solution in a 150 mL PE plastic beaker covered with PE film. After being stirred at a rate of 300 rpm for a specified time, the solution was immediately filtered through 0.22 μm syringe filters (Millipore Millex). The fluoride concentrations of the filtrates were determined by ion chromatography. For breakthrough studies of fluoride removal, batch adsorption method was adopted. The initial fluoride concentration was 5 mg L^{-1} and the initial pH value was 6.5. During the test, 1.0 g of adsorbents was added to a series of fluoride solution ranging from 1 L to 20 L under stirring at a rate of 300 rpm. After stirred for 12 h, the equilibrium concentration of each fluoride solution with different volumes was measured to determine the breakthrough point based on the guideline value set by the WHO.

The stock solution of As (V) was prepared using $Na_2HAsO_4{\cdot}7H_2O$ and the stock solution of As (III) was prepared with $NaAsO_2$. The initial As (V) concentrations of the test solutions were 100 and 200 ppb, respectively. The initial As (III) concentration was fixed at 100 ppb. The pH values of all arsenic solution were 7 ± 0.2 without any adjustments and no buffer was used. The amount of adsorbents was fixed at 1.0 g for each adsorption experiment. The volumes of arsenic solution were varied from 20 to 300 L to monitor the change of arsenic equilibrium concentration. All the arsenic adsorption tests were carried out at 298 K under stirring at a rate of 300 rpm for 12 h and then the equilibrium arsenic concentrations were measured by inductively coupled plasma atomic emission spectroscopy (ICP-AES). All the adsorption experiments were repeated three times and the mean values were reported.

2.4. Characterization

The microscopic features of the samples were characterized by transmission electron microscopy (TEM, FEI Tecnai F20). X-ray powder diffraction (XRD) patterns and small-angle X-ray powder diffraction patterns were recorded on a Rigaku D/max-2500 diffractometer with Cu KR radiation (λ = 0.1542 nm) at 40 kV and 200 mA. For the XPS analysis, a Kratos AXIS 165 multitechnique electron spectrometer was utilized. The nitrogen adsorption and desorption isotherms at 78.3 K were measured using a Quantachome AS-1 analyzer. All the samples were outgassed under vacuum at 200 °C for 3 h prior to measurement. Energy Dispersive X-ray Analysis (EDXA) was carried out using Energy Dispersive X-ray Spectroscopy detector (Oxford INCA). The concentration of fluoride was determined by ion chromatography (IC Dionex ICS-900) equipped with a Dionex AS 14A analytical column and a DS5 conductivity detector. The eluent is 3.5 mM of Na_2CO_3 and 1 mM of $NaHCO_3$ mixed solution and its flow rate is 1 mL min^{-1}. The injection volume of samples is 10 μL. The operating temperature is 298 K. The concentrations of As and Al were measured by inductively coupled plasma atomic emission spectroscopy (ICP-AES, Shimadzu ICPE-9000).

3. Results and discussion

3.1. Characterization of adsorbents

As shown in Fig. 1, TEM images confirm the presence of highly uniform and hexagonally ordered mesopores with p6mm symmetry on all samples [43]. The cylindrical pores along [1 1 0] direction and hexagonal pore openings along [0 0 1] direction from the meso-Al-400 sample are shown in Fig. 1a and b, respectively. Fig. 1c shows that the Ca-doped mesoporous alumina (meso-Al-10Ca-400) also possesses similar ordered pore networks and highly uniform channels. The TEM image of sample meso-Al-900 (Fig. 1d) indicates that the ordered mesoporous framework is preserved after calcination at 900 °C. More TEM images (Fig. S1a and b in Supplementary material) show similar highly order pore networks of other samples.

X-ray diffraction (XRD) patterns of these samples (Fig. 2a) demonstrate that both mesoporous aluminas and Ca-doped aluminas calcined at 400 °C are composed of amorphous walls, which can be converted into γ-Al_2O_3 phase (JCPDS Card No. 10-0425) after further treatment at 900 °C. Small-angle XRD patterns of samples calcined at 400 °C (the inset of Fig. 2a) confirm the formation of relatively ordered mesopores. Sample meso-Al-400 shows a diffraction peak around 1.2°, and the diffraction peak of sample meso-Al-10Ca-400 shifts to around 1.4°. The presence of calcium on sample meso-Al-10Ca-400 is confirmed by X-ray photoelectron spectroscopy (XPS, Fig. S2 shown in Supplementary material),

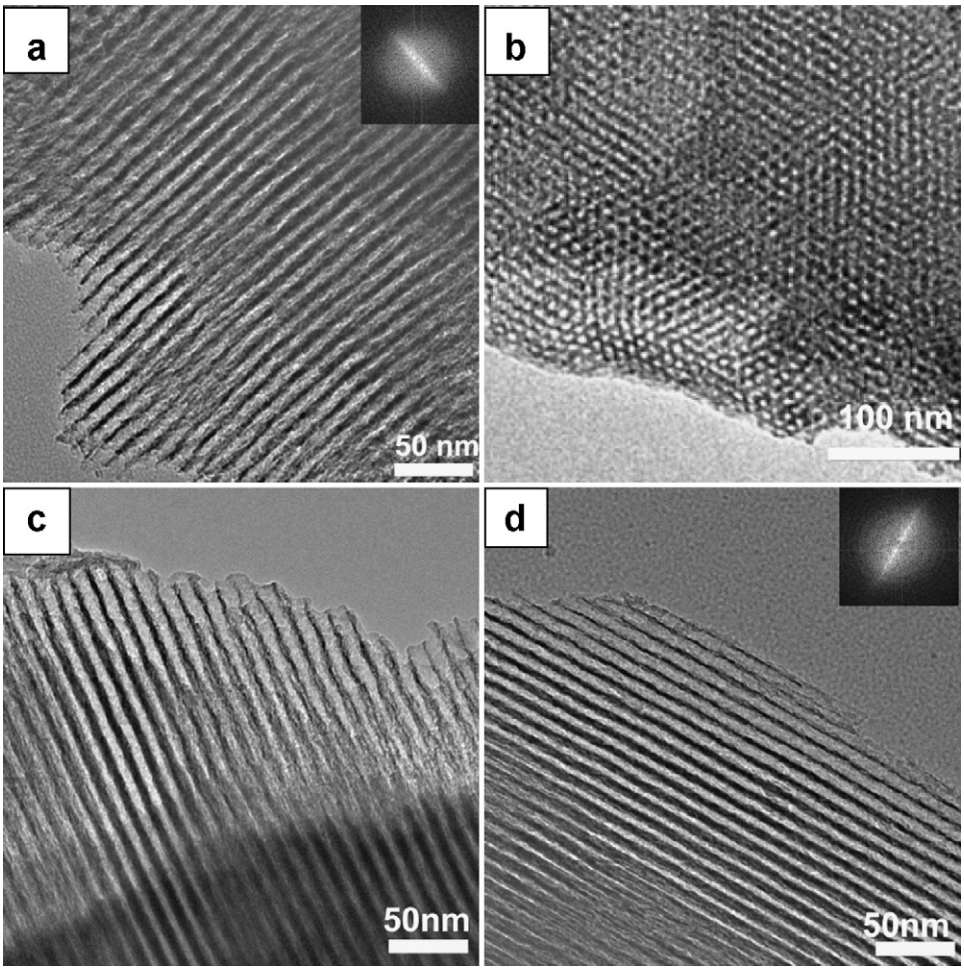

Fig. 1. (a) and (b) TEM images of meso-Al-400 viewed along [1 1 0] and [0 0 1] orientation, respectively (the inset of 1a is fast Fourier transform (FFT) diffractogram); (c) TEM image of meso-Al-10Ca-400 viewed along [1 1 0] direction; (d) TEM image of meso-Al-900 viewed along [1 1 0] orientation (the inset of 1d is FFT diffractogram).

which shows calcium 2p peak at the binding energy of 347.5 eV, which agrees well with the EDXA results (Fig. S3 in Supplementary material).

Nitrogen adsorption–desorption isotherms of various mesoporous aluminas and Ca-doped aluminas are shown in Fig. 2b and c. All isotherms are type IV curves with H1-shaped hysteresis loops. Table 1 summarizes the Brumauer–Emmett–Teller (BET) surface areas, pore sizes and pore volumes of various mesoporous aluminas and Ca-doped aluminas. The large surface areas (i.e., high density of adsorption sites) and uniform mesoporous structure with well-defined channels on these samples will enhance their adsorption abilities in the water treatment.

The pH values of zero point of charge (pH_{zpc}) of these prepared adsorbents are listed in Table S1 in Supplementary material. The pH value of the aqueous solution plays a significant role in the surface charge of the adsorbent which determines the adsorption performance. Based on the pH_{zpc} values of the adsorbents, the initial pH value of all adsorption tests is between 6.5 and 7. The adsorbents are positively charged in this pH range, which is favorable for the adsorption of anions.

Table 1
Porous characteristics of various order mesoporous aluminas.

Sample	BET surface area ($m^2\ g^{-1}$)	Pore size (nm)	Pore volume ($cm^3\ g^{-1}$)
Meso-Al-400	361	3.8	0.957
Meso-Al-900	237	5.6	0.511
Meso-Al-5Ca-400	279	6.6	0.73
Meso-Al-10Ca-400	280	6.6	0.77

3.2. Kinetics and equilibrium adsorption isotherms for fluoride ions

Fig. 3a reveals the adsorption rate of fluoride ions on the as-prepared meso-Al-400 samples, when 0.01 g of meso-Al-400 sample was added to 100 mL of fluoride ion solution with an initial concentration of 10 mg L^{-1}. The adsorption process is fast during the first 60 min and the equilibrium is established after 5 h. In order to ensure that the adsorption equilibrium is reached, 12 h is fixed as the contact time for further adsorption studies. Based on the amount of fluoride ions being removed, the fluoride removal capacity was calculated to be 39 mg/g with an initial fluoride concentration of 10 ppm. This defluoridation capacity at a relatively low initial concentration of 10 ppm is significantly higher than the reported results of activated alumina, hydroxyapatite, lime or bone char [1,2,25,33,34,45].

In order to further investigate the adsorption process, adsorption isotherms are obtained with initial fluoride concentrations ranging from 2 to 1000 mg L^{-1}. Fig. 3b exhibits the adsorption isotherms of fluoride ion over various samples including highly ordered mesoporous aluminas and Ca-doped aluminas.

Several models have been established to describe the experimental data of adsorption isotherms [46,47]. Among them, the Langmuir [48] and Freundlich [49] models are most frequently used

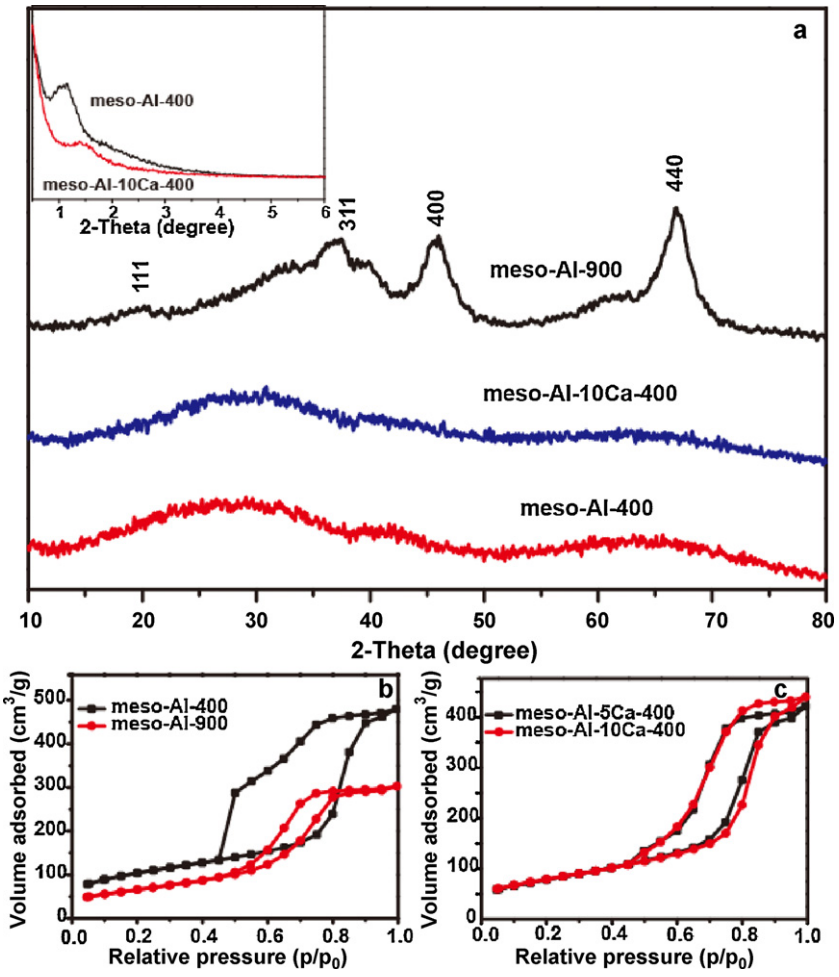

Fig. 2. (a) XRD patterns of mesoporous aluminas and Ca doped aluminas (the inset is small-angle XRD patterns of mesoporous aluminas and Ca doped aluminas); (b) and (c) nitrogen adsorption and desorption isotherms of mesoporous aluminas and Ca-doped aluminas, respectively.

for adsorption analysis. The Langmuir model can be described as following [48]:

$$q_e = \frac{q_m b C_e}{1 + bC_e} \quad (1)$$

where C_e is the equilibrium concentration of fluoride ions (mg L^{-1}), q_e is the amount of fluoride adsorbed per unit weight of the adsorbent at equilibrium (mg/g), q_m (mg/g) is the maximum adsorption capacity corresponding to complete monolayer coverage and b is the equilibrium constant related to the energy.

The Freundlich model is an empirical description of adsorption on heterogeneous surface [49]. The Freundlich equation can be described as following:

$$q_e = K_F C_e^{1/n} \quad (2)$$

where C_e is the equilibrium concentration of fluoride ions (mg L^{-1}), q_e is the amount of fluoride adsorbed per unit weight of the adsorbent at equilibrium (mg/g), K_F is the empirical constant (L mg^{-1}) and n is the empirical parameter related to the adsorption intensity.

The full adsorption isotherms of fluoride ion on the meso-Al-400, meso-Al-900, meso-Al-5Ca-400, and meso-Al-10Ca-400 cannot be well-fitted with either Langmuir or Freundlich models at the whole wide range of fluoride concentrations. However, the experimental data with fluoride concentrations below 150 mg L^{-1} could be well fitted with the Langmuir adsorption isotherm as shown in the inset of Fig. 3b. These results suggest that the removal of fluoride ions may be due to monolayer adsorption onto the positively charged surface of adsorbents at low initial fluoride ion concentrations (below 150 ppm). However, at higher initial concentrations, fluoride ions may be removed through different routes, likely chemical reactions.

When the initial concentration of fluoride ion is below 100 mg L^{-1}, meso-Al-400 has higher adsorption capacity than those of the other three samples due to its higher BET surface area value. Samples calcined at 400 °C with amorphous pore walls show much higher fluoride adsorption capacities than that of the samples calcined at 900 °C (meso-Al-900). In addition, the Ca-doped mesoporous alumina samples exhibit higher fluoride removal capacity than those of pure mesoporous aluminas at higher initial fluoride concentrations, probably because calcium ions may react with fluoride ions to form CaF_2 precipitates, which provides another route to remove more fluoride. At the initial fluoride concentration of 1000 ppm, the removal capacity of meso-Al-10Ca-400 reaches 450 mg/g, which is about 60 times higher than that of commercial activated alumina (ca. 7 mg/g) [25].

3.3. Breakthrough studies of fluoride removal

The fluoride concentration in contaminated groundwater is usually less than 10 ppm. Thus the defluoridation capacity at lower fluoride concentrations is perhaps a more important feature for fluoride removal materials. In a series of experiments, we fixed the amount of meso-Al-400 at 1.0 g and the initial concentration of fluoride at 5 ppm, and varied the volume of fluoride solutions from 1

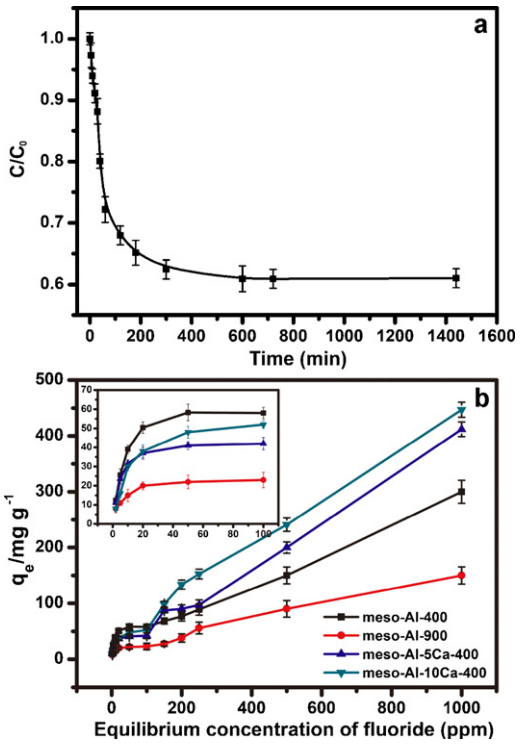

Fig. 3. (a) Time dependant concentration of fluoride ions in aqueous solution treated with meso-Al-400 with initial fluoride concentration of 10 ppm (the stirring rate is 300 rpm; the initial pH value of fluoride solution is 6.5 and the equilibrium pH is between 6.8 and 7.1); and (b) adsorption isotherms of fluoride over various samples at 298 K. (The inset is the magnified section from 0 to 100 ppm. The stirring rate is 300 rpm; the initial pH value of various fluoride solutions is set at 6.5 and the equilibrium pH is between 6.8 and 8.0.)

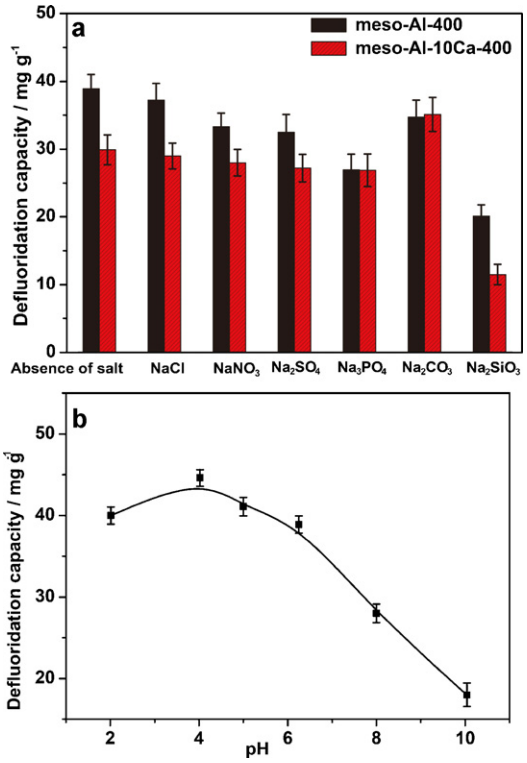

Fig. 4. (a) Effect of co-existing anions on defluoridation capacity of meso-Al-400 (The initial concentration of fluoride is 10 ppm; the initial concentration of competing anions including Cl^- and SO_4^{2-} are 200 ppm; the initial concentration of NO_3^- is 10 ppm and the initial concentration of PO_4^{3-}, CO_3^{2-} and SiO_3^{2-} is 50 ppm. The initial pH of all solutions is fixed at 6.5. The equilibrium pH falls in the range between 7.01 and 7.67.) and (b) influence of initial pH on fluoride adsorption with meso-Al-400 (the initial concentration of fluoride is 10 ppm). The stirring rate in this part of tests is fixed at 300 rpm.

to 20 L to monitor the change of fluoride concentration. The results are listed in Table 2. The equilibrium concentration rises with the increasing amount of fluoride solution. Since the guideline value set by the WHO is 1.5 mg L^{-1}, we define the amount of treated water when the fluoride concentration of output water reaches 1.5 ppm as the breakthrough point. Table 2 shows that 1 g of the meso-Al-400 adsorbent can deal with about 4 L of water containing 5 ppm of fluoride before the breakthrough point is reached. Moreover the concentration of aluminum in treated water is only about 20 ppb, indicating that the adsorption treatment with these mesoporous aluminas will not bring secondary aluminum contamination.

3.4. Effect of co-existing anions and pH value

Natural fluoride-contaminated underground water always contains other anions such as Cl^-, SO_4^{2-} and PO_4^{3-} which may compete with fluoride for the active adsorption sites. Six solutions containing 200 ppm of Cl^-, 10 ppm of NO_3^-, 200 ppm of SO_4^{2-}, 50 ppm of PO_4^{3-}, 50 ppm of CO_3^{2-} and 50 ppm of SiO_3^{2-}, respectively, were prepared with an initial fluoride concentration of 10 ppm. Fig. 4a depicts the effect of various co-existing anions on the defluoridation capacity of meso-Al-400 and meso-Al-10Ca adsorbents. There is no substantial influence on the overall defluoridation capacity of meso-Al-400 and meso-Al-10Ca samples in the presence of Cl^-, NO_3^-, SO_4^{2-} and CO_3^{2-}. At the pH of 6.5, carbonate mainly exists in the form of HCO_3^-. Previous studies indicated that HCO_3^- had little impact or even positive effect on the fluoride adsorption sometimes [1,50]. SO_4^{2-} has a relatively greater negative effect on fluoride adsorption because of its higher negative charge compared to that of Cl^- and NO_3^- [39,51]. Both phosphate and silicate affect the fluoride sorption of adsorbents significantly, because they have higher negative charge and relatively high affinity to aluminum-based adsorbents, resulting in the adverse effect on fluoride removal [7,52]. The defluoridation capacity of meso-Al-400 declines by 30.7% and 48% in the presence of PO_4^{3-} and SiO_3^{2-}, respectively. However, the adsorbent of meso-Al-400 still maintains high fluoride removal capacities (more than 20 mg/g) in the presence of most of anions, indicating excellent selectivity towards fluoride.

The pH value of the aqueous solution determines the surface charge of the adsorbents [53,54]. The adsorption of fluoride on the meso-Al-400 was examined at different initial pH values ranging from 2 to 10 (Fig. 4b). In aqueous solution, the adsorption process is primarily governed by the zero point charge (ZPC) of an adsorbent. Typically, ZPC values for alumina fall in a range of pH 8–10 [2]. The pH_{zpc} values for the adsorbents in this study also fall in this range. The higher defluoridation capacity in acidic medium can be assigned to the gradual increase in attraction between positively

Table 2
Equilibrium concentration of fluoride ions with different amounts of treated water.

Volume (L g^{-1})	1	2	4	5	8	10	20
Equilibrium concentration of F^- (ppm)	0.13	0.51	1.5	1.59	2.31	2.44	3.4

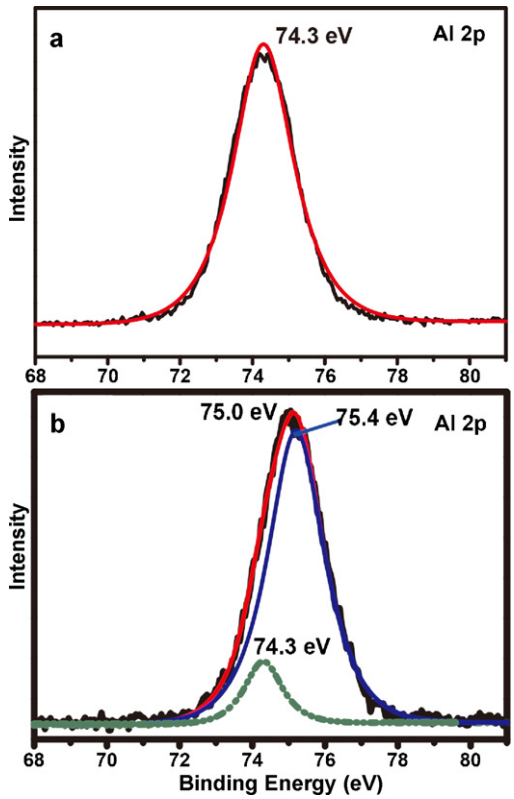

Fig. 5. XPS spectra for meso-Al-400 (a) before and (b) after adsorption (adsorbent dose = 0.1 g/L, initial concentration of fluoride is 1000 ppm).

charged surface of adsorbents and negatively charged fluoride ions. However, in the strong acidic pH region (pH < 4) the alumina will be partially dissolved, resulting in the decrease of fluoride adsorption capacity [1,29,54].

3.5. Mechanism of fluoride adsorption

In order to investigate the interaction between fluoride and aluminum, XPS spectra (Al 2p) for meso-Al-400 before and after fluoride adsorption are obtained. As shown in Fig. 5a, only one Al 2p peak is observed at 74.3 eV from fresh meso-Al-400 sample, indicating that its amorphous structure is similar to pseudoboehmite (AlOOH) [55,56]. After fluoride adsorption, the Al 2p peak position shifts to 75.0 eV and becomes broader. It could be convoluted into two peaks (74.3 eV and 75.4 eV). The Al 2p peak at 74.3 eV is attributed to aluminum in meso-Al-400 as mentioned above, and the new peak at 75.4 eV can be assigned to aluminum atoms that bonded with fluoride. The area of the Al 2p peak at 75.4 eV is much larger than that of the peak at 74.3 eV, suggesting that most of the surface Al atoms participate in the adsorption of fluoride. Besides the presence of this new Al 2p peak, a new F 1s peak at 686 eV (Fig. S4) is also observed after fluoride adsorption [57]. The XPS results are consistent with the ligand exchange adsorption mechanism reported by previous researchers [1,25,58]. Such ligand exchange mechanism can be briefly illustrated as:

$$=Al–OH + H^+ + F^- \leftrightarrow =Al–F + H_2O \quad (3)$$

The EDXA spectra of the fluoride adsorbed mesoporous alumina (meso-Al-400) shown in Fig. S5, confirming the existence of fluoride species adsorbed on the adsorbent. In addition, some of sodium ions are also absorbed on the mesoporous aluminas.

3.6. Comparison with other adsorbents and cost analysis

As mentioned in Section 1, there are several defluoridation and arsenic removal methods including chemical precipitation, ion exchange, membrane process, adsorption technique and electrodialysis. The adsorption technique is perhaps most suitable for households or small villages, where simplicity and low cost are especially desirable. The simplest adsorption unit may require only a filter. A wide variety of adsorbents have been reported for fluoride removal. The maximum adsorption capacities of prepared adsorbents of meso-Al-10Ca-400 and meso-Al-400 are compared with those of other adsorbents reported in the literatures. As shown in Table 3, the maximum removal capacity of meso-Al-400 or meso-Al-10Ca-400 is significantly higher than those of other adsorbents. These results show that these ordered mesoporous aluminas own high defluoridation capacity. At lab fabrication scale, the cost of these mesoporous aluminas is high compared to commercial adsorbents. However, with intensive follow-up studies to develop the low-cost method at scaled up production level, the cost of these materials can be lowered to be comparable with commercial adsorbents.

3.7. Arsenic removal

These ordered mesoporous aluminas are superb materials for arsenic removal. In this study, we focus on the arsenic removal capacity at low arsenic concentrations. This is because the arsenic concentration of contaminated groundwater is usually less than 200 ppb. Similar to the fluoride adsorption process, the initial pH value of the arsenic aqueous solution influences the arsenic removal performance significantly. Therefore, it is essential to study the effect of initial pH values on the removal of arsenic at a lower concentration. The adsorption of arsenate on the meso-Al-400 was examined at different pH values ranging from 2 to 13 by setting the initial concentration of As (V) at 500 ppb. The meso-Al-400 adsorbent was stirred in the arsenate solution at a rate of 300 rpm for 12 h and then the equilibrium concentrations of As (V) and Al in the residual solution were measured to determine the removal efficiency of arsenate and the degree of dissolution of aluminum. Fig. 6 reveals the effect of initial pH on the removal of arsenate ions, showing that the arsenic removal is strongly pH dependent. The mesoporous alumina can remove arsenate ions efficiently in the initial pH range of 4–9. Meanwhile, the

Table 3
Comparison of the maximum fluoride adsorption capacity with published data.

Adsorbent	pH	Initial F^- concentration range (mg L^-)	Contact time (h)	Adsorbent dosage (g/L)	Temperature (K)	Adsorption capacity (mg/g)	Reference
Meso-Al-10Ca-400	6.5	2–1000	12	0.1	298	450	This work
Meso-Al-400	6.5	2–1000	12	0.1	298	300	This work
Activated alumina	5.2	10–50	16	5	303	7.6	[25]
CaO modified activated alumina	5.5	1–1000	48	6.67	298	96.23	[27]
Mixed rare earth oxides	6.5	1–50	1	4	302	196.08	[34]
Zeolite	5.2	10–80	24	2	313	39.5	[39]
Activated carbon	2.0	1–20	3	2	298	15.9	[51]

Table 4
Equilibrium concentration of As (V) with different amount of treated water.

Volume of arsenic-contained water (L g^{-1})	Initial concentration of As (V) (ppb)	Equilibrium concentration of As (V) after adsorption (ppb)	Initial concentration of As (V) (ppb)	Equilibrium concentration of As (V) after adsorption (ppb)
20	100	Not detected	200	Not detected
50	100	Not detected	200	Not detected
100	100	1	200	1
200	100	1.2	200	55.5
300	100	20	200	120

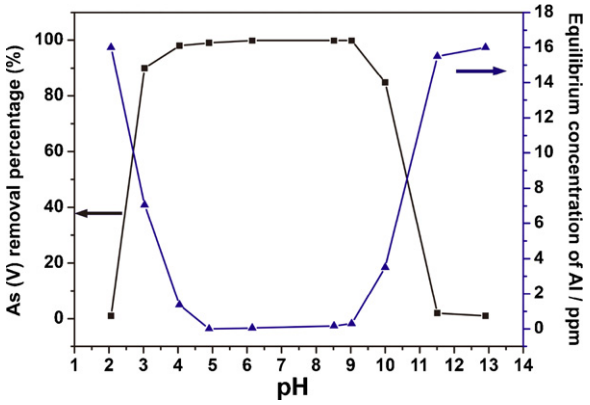

Fig. 6. Impact of initial pH values on arsenate removal with meso-Al-400 and the dissolution amount of meso-Al-400 adsorbents (the stirring rate is 300 rpm).

concentration of aluminum is very low, indicating that the as-prepared mesoporous alumina is stable in this pH range.

The breakthrough point of meso-Al-400 adsorbents was measured with initial arsenate concentrations of 100 and 200 ppb, respectively. The initial pH value of the arsenate solution is 7.0 without pH adjustment. The breakthrough point was set when the concentration of arsenate exceeded 10 ppb. As shown in Table 4, the equilibrium concentration of arsenate rises with the increasing volume of treated water. At the breakthrough point, 1 g of sample meso-Al-400 can treat about 200 L of water containing 100 ppb of arsenate, indicating that its arsenic adsorption capacity is 19.8 mg/g at a low initial arsenic concentration. Again, the concentration of aluminum in treated water is only about 20 ppb. Such a high arsenic adsorption capacity at low arsenic concentrations makes these ordered mesoporous aluminas ideal candidates in practical arsenate removal units.

Moreover, the removal of As (III) with these highly ordered mesoporous aluminas was also tested considering that arsenite also exists in natural groundwater and is considerably more toxic than arsenate [12,36,41]. As shown in Table 5, the equilibrium concentration of As (III) grows up with the rising volume of treated water. At the breakthrough point, 1 g of sample meso-Al-400 can treat 50 L of water containing 100 ppb of arsenite, indicating that its As (III) adsorption capacity is 5 mg/g at such a low initial concentration. Arsenite is more difficult to be removed than arsenate. The results in this study agree with many previous reports [4,11–13,36,41]. In addition, As (III) can be converted to As (V) before adsorption in practical water treatment.

Table 5
Equilibrium concentration of As (III) with different amount of treated water.

Volume of arsenic-contained water (L g^{-1})	Initial concentration of As (III) (ppb)	Equilibrium concentration of As (III) after adsorption (ppb)
20	100	Not detected
50	100	8
100	100	40
200	100	75
300	100	85

The adsorption rate is also important to evaluate the adsorbents. When 5 g of meso-Al-400 was added into 1000 g of water with an initial arsenate concentration of 100 ppb, the arsenate concentration can be reduced to below 10 ppb in less than 2 min. It has been reported that activated alumina required 48 h to reach the equilibrium, and mesoporous γ-alumina needed 5 h to reach the equilibrium under similar conditions [26,41]. The adsorption kinetics on meso-Al-400 is assisted by the uniform and well-defined pore structure that provides easily accessible adsorption sites, and faster transportation routes for arsenic species.

4. Conclusions

We produced highly ordered mesoporous aluminas and Ca-doped aluminas through a reproducible and high yield sol–gel method. Fluoride adsorption tests demonstrated that they had excellent defluoridation capacities and selectivity towards fluoride in the presence of competing anions. The highest fluoride removal capacity reached 450 mg/g. These highly ordered mesoporous aluminas also exhibited superb arsenic removal capacities and adsorption kinetics. 1 g of sample meso-Al-400 can treat 200 L of arsenic contaminated water, reducing the arsenic concentration from 100 ppb to less than 10 ppb, suggesting that these ordered mesoporous aluminas can be the ideal adsorbents in the practical water treatment application.

Acknowledgements

We thank the financial supports from the National Natural Science Foundation of China (NSFC 50725207, 20821003), National Basic Research Program of China (2009CB930400, 2011CB933700) and the Chinese Academy of Sciences.

Appendix A. Supplementary data

Supplementary data associated with this article can be found, in the online version, at doi:10.1016/j.jhazmat.2011.10.025.

References

[1] S.G. Wang, Y. Ma, Y.J. Shi, W.X. Gong, Defluoridation performance and mechanism of nano-scale aluminum oxide hydroxide in aqueous solution, J. Chem. Technol. Biotechnol. 84 (2009) 1043–1050.
[2] G. Lee, C. Chen, S.T. Yang, W.S. Ahn, Enhanced adsorptive removal of fluoride using mesoporous alumina, Microporous Mesoporous Mater. 127 (2010) 152–156.
[3] D. Mohan, J.C.U. Pittman, Arsenic removal from water/wastewater using adsorbents – a critical review, J. Hazard. Mater. 142 (2007) 1–53.
[4] B.K. Mandal, K.T. Suzuki, Arsenic round the world: a review, Talanta 58 (2002) 201–235.
[5] M. Berg, H.C. Tran, T.C. Nguyen, H.V. Pham, R. Schertenleib, W. Giger, Arsenic contamination of groundwater and drinking water in Vietnam: a human health threat, Environ. Sci. Technol. 35 (2001) 2621–2626.
[6] A.L. Rose, T.D. Waite, Kinetic model for Fe(II) oxidation in seawater in the absence and presence of natural organic matter, Environ. Sci. Technol. 36 (2002) 433–444.
[7] M. Mohapatra, S. Anand, B.K. Mishra, D.E. Giles, P. Singh, Review of fluoride removal from drinking water, J. Environ. Manage. 91 (2009) 67–77.

[8] S. Saha, Treatment of aqueous effluent for fluoride removal, Water Res. 27 (1993) 1347–1350.
[9] P.L. Bishop, G. Sansoucy, Fluoride removal from drinking-water by fluidized acticated alumina adsorption, J. Am. Water Works Assoc. 70 (1978) 554–559.
[10] E.J. Reardon, Y. Wang, A limestone reactor for fluoride removal from wastewaters, Environ. Sci. Technol. 34 (2000) 3247–3253.
[11] A. Violante, M. Ricciardella, S. Del Gaudio, M. Pigna, Coprecipitation of arsenate with metal oxides: nature, mineralogy, and reactivity of aluminum precipitates, Environ. Sci. Technol. 40 (2006) 4961–4967.
[12] A. Violante, S.D. Gaudio, M. Pigna, M. Ricciardella, D. Banerjee, Coprecipitation of arsenate with metal oxides: 2. Nature, mineralogy, and reactivity of iron(III) precipitates, Environ. Sci. Technol. 41 (2007) 8275–8280.
[13] A. Violante, M. Pigna, S. Del Gaudio, V. Cozzolino, D. Banerjee, Coprecipitation of arsenate with metal oxides: 3. Nature, mineralogy, and reactivity of iron(III)–aluminum precipitates, Environ. Sci. Technol. 43 (2009) 1515–1521.
[14] K. Vaaramaa, J. Lehto, Removal of metals and anions from drinking water by ion exchange, Desalination 155 (2003) 157–170.
[15] C. Castel, M. Schweizer, M.O. Simonnot, M. Sardin, Selective removal of fluoride ions by a two-way ion-exchange cyclic process, Chem. Eng. Sci. 55 (2000) 3341–3352.
[16] K. Hu, J.M. Dickson, Nanofiltration membrane performance on fluoride removal from water, J. Membr. Sci. 279 (2006) 529–538.
[17] S. Joshi, S. Mehta, A. Rao, A. Rao, Estimation of sodium fluoride using HPLC in reverse osmosis experiments, Water Treat. 7 (1992) 207–210.
[18] M.d.L. Ballinas, E.M.T. Rodríguez de San Miguel, d.J. Rodríguez, O. Silva, M. Muñoz, J. de Gyves, Arsenic(V) removal with polymer inclusion membranes from sulfuric acid media using DBBP as carrier, Environ. Sci. Technol. 38 (2003) 886–891.
[19] Y.-H. Weng, L.H. Chaung-Hsieh, H.-H. Lee, K.-C. Li, C.P. Huang, Removal of arsenic and humic substances (HSs) by electro-ultrafiltration (EUF), J. Hazard. Mater. 122 (2005) 171–176.
[20] S. Gao, R. Sun, Z. Wei, H. Zhao, H. Li, F. Hu, Size-dependent defluoridation properties of synthetic hydroxyapatite, J. Fluorine Chem. 130 (2009) 550–556.
[21] A. Bhatnagar, E. Kumar, M. Sillanpää, Fluoride removal from water by adsorption – a review, Chem. Eng. J. 171 (2011) 811–840.
[22] M. Hichour, F. Persin, J. Sandeaux, C. Gavach, Fluoride removal from waters by Donnan dialysis, Sep. Purif. Technol. 18 (2000) 1–11.
[23] T. Ruiz, F. Persin, M. Hichour, J. Sandeaux, Modelisation of fluoride removal in Donnan dialysis, J. Membr. Sci. 212 (2003) 113–121.
[24] Z. Amor, B. Bariou, N. Mameri, M. Taky, S. Nicolas, A. Elmidaoui, Fluoride removal from brackish water by electrodialysis, Desalination 133 (2001) 215–223.
[25] Y. Ku, H. Chiou, The adsorption of fluoride ion from aqueous solution by activated alumina, Water Air Soil Pollut. 133 (2002) 349–361.
[26] T. Lin, J. Wu, Adsorption of arsenite and arsenate within activated alumina grains: equilibrium and kinetics, Water Res. 35 (2001) 2049–2057.
[27] L.M. Camacho, A. Torres, D. Saha, S. Deng, Adsorption equilibrium and kinetics of fluoride on sol–gel-derived activated alumina adsorbents, J. Colloid Interface Sci. 349 (2010) 307–313.
[28] W. Choi, K. Chen, The removal of fluoride from waters by adsorption, J. Am. Water Works Assoc. 71 (1979) 562–570.
[29] C. Sundaram, N. Viswanathan, S. Meenakshi, Defluoridation chemistry of synthetic hydroxyapatite at nano scale: equilibrium and kinetic studies, J. Hazard. Mater. 155 (2008) 206–215.
[30] P. Pommerenk, G. Schafran, Effects of prefluoridation on removal of particles and organic matter, J. Am. Water Works Assoc. 94 (2002) 99–108.
[31] M. Islam, R. Patel, Evaluation of removal efficiency of fluoride from aqueous solution using quick lime, J. Hazard. Mater. 143 (2007) 303–310.
[32] Y. engelolu, E. KIr, M. Ers z, Removal of fluoride from aqueous solution by using red mud, Sep. Purif. Technol. 28 (2002) 81–86.
[33] L. Brunson, D. Sabatini, An evaluation of fish bone char as an appropriate arsenic and fluoride removal technology for emerging regions, Environ. Eng. Sci. 26 (2009) 1777–1784.
[34] A. Raichur, M. Jyoti Basu, Adsorption of fluoride onto mixed rare earth oxides, Sep. Purif. Technol. 24 (2001) 121–127.
[35] T. Nguyen, S. Vigneswaran, H. Ngo, J. Kandasamy, Arsenic removal by Iron oxide coated sponge: experimental performance and mathematical models, J. Hazard. Mater. 182 (2010) 723–729.
[36] K. Raven, A. Jain, R. Loeppert, Arsenite and arsenate adsorption on ferrihydrite: kinetics, equilibrium, and adsorption envelopes, Environ. Sci. Technol. 32 (1998) 344–349.
[37] K. Goh, T. Lim, Z. Dong, Enhanced arsenic removal by hydrothermally treated nanocrystalline Mg/Al layered double hydroxide with nitrate intercalation, Environ. Sci. Technol. 43 (2009) 2537–2543.
[38] Y. Xu, Y. Dai, J. Zhou, Z. Xu, G. Qian, G. Lu, Removal efficiency of arsenate and phosphate from aqueous solution using layered double hydroxide materials: intercalation vs. precipitation, J. Mater. Chem. 20 (2010) 4684–4691.
[39] M. Onyango, Y. Kojima, O. Aoyi, E. Bernardo, H. Matsuda, Adsorption equilibrium modeling and solution chemistry dependence of fluoride removal from water by trivalent-cation-exchanged zeolite F-9, J. Colloid Interface Sci. 279 (2004) 341–350.
[40] S.-W. Bian, Z. Ma, L.-S. Zhang, F. Niu, W.-G. Song, Silica nanotubes with mesoporous walls and various internal morphologies using hard/soft dual templates, Chem. Commun. (2009) 1261–1263.
[41] Y. Kim, C. Kim, I. Choi, S. Rengaraj, J. Yi, Arsenic removal using mesoporous alumina prepared via a templating method, Environ. Sci. Technol. 38 (2004) 924–931.
[42] S. Morris, P. Fulvio, M. Jaroniec, Ordered mesoporous alumina-supported metal oxides, J. Am. Chem. Soc. 130 (2008) 15210–15216.
[43] Q. Yuan, A.-X. Yin, C. Luo, L.-D. Sun, Y.-W. Zhang, W.-T. Duan, H.-C. Liu, C.-H. Yan, Facile synthesis for ordered mesoporous γ-aluminas with high thermal stability, J. Am. Chem. Soc. 130 (2008) 3465–3472.
[44] S.-W. Bian, Y.-L. Zhang, H.-L. Li, Y. Yu, Y.-L. Song, W.-G. Song, Alumina with hierarchically ordered mesopore/macropore from dual templates, Microporous Mesoporous Mater. 131 (2010) 289–293.
[45] B.D. Turner, P. Binning, S.L.S. Stipp, Fluoride removal by calcite: evidence for fluorite precipitation and surface adsorption, Environ. Sci. Technol. 39 (2005) 9561–9568.
[46] L. Zhong, J. Hu, H. Liang, A. Cao, W. Song, L. Wan, Self-assembled 3D flowerlike iron oxide nanostructures and their application in water treatment, Adv. Mater. 18 (2006) 2426–2431.
[47] L. Zhong, J. Hu, A. Cao, Q. Liu, W. Song, L. Wan, 3D flowerlike ceria micro/nanocomposite structure and its application for water treatment and CO removal, Chem. Mater. 19 (2007) 1648–1655.
[48] I. Langmuir, The constitution and fundamental properties of solid and liquids. Part I. Solids, J. Am. Chem. Soc. 38 (1916) 2221–2295.
[49] H. Freundlich, Tiber die adsorption in Losungen, Z. Phys. Chem. 57 (1906) 385–470.
[50] S.M. Maliyekkal, S. Shukla, L. Philip, I.M. Nambi, Enhanced fluoride removal from drinking water by magnesia-amended activated alumina granules, Chem. Eng. J. 140 (2008) 183–192.
[51] A.A.M. Daifullah, S.M. Yakout, S.A. Elreefy, Adsorption of fluoride in aqueous solutions using $KMnO_4$-modified activated carbon derived from steam pyrolysis of rice straw, J. Hazard. Mater. 147 (2007) 633–643.
[52] S. Tanada, M. Kabayama, N. Kawasaki, T. Sakiyama, T. Nakamura, M. Araki, T. Tamura, Removal of phosphate by aluminum oxide hydroxide, J. Colloid Interface Sci. 257 (2003) 135–140.
[53] O. Hao, C. Huang, Adsorption characteristics of fluoride onto hydrous alumina, J. Environ. Eng. 112 (1986) 1054–1069.
[54] P. Pommerenk, G. Schafran, Adsorption of inorganic and organic ligands onto hydrous aluminum oxide: evaluation of surface charge and the impacts on particle and NOM removal during water treatment, Environ. Sci. Technol. 39 (2005) 6429–6434.
[55] S. Thomas, P. Sherwood, Valence band spectra of aluminum oxides, hydroxides, and oxyhydroxides interpreted by X. alpha. calculations, Anal. Chem. 64 (1992) 2488–2495.
[56] J. Kloprogge, L. Duong, B. Wood, R. Frost, XPS study of the major minerals in bauxite: Gibbsite, bayerite and (pseudo-) boehmite, J. Colloid Interface Sci. 296 (2006) 572–576.
[57] O. Boese, W. Unger, E. Kemnitz, S. Schroeder, Active sites on an oxide catalyst for F/Cl-exchange reactions: X-ray spectroscopy of fluorinated γ-Al_2O_3, Phys. Chem. Chem. Phys. 4 (2002) 2824–2832.
[58] A. López Valdivieso, J.L. Reyes Bahena, S. Song, R. Herrera Urbina, Temperature effect on the zeta potential and fluoride adsorption at the α-Al_2O_3/aqueous solution interface, J. Colloid Interface Sci. 298 (2006) 1–5.